A Microfluidic Cancer-on-Chip Platform Predicts Drug Response Using Organotypic Tumor Slice Culture

Sanjiban Chakrabarty[1,2], William F. Quiros-Solano[3,4], Maayke M.P. Kuijten[1,5], Ben Haspels[1], Sandeep Mallya[6], Calvin Shun Yu Lo[1], Amr Othman[4], Cinzia Silvestri[4], Anja van de Stolpe[7], Nikolas Gaio[4], Hanny Odijk[1], Marieke van de Ven[8], Corrina M.A. de Ridder[9], Wytske M. van Weerden[9], Jos Jonkers[8], Ronald Dekker[3,7], Nitika Taneja[1], Roland Kanaar[1,5], and Dik C. van Gent[1,5]

ABSTRACT

Optimal treatment of cancer requires diagnostic methods to facilitate therapy choice and prevent ineffective treatments. Direct assessment of therapy response in viable tumor specimens could fill this diagnostic gap. Therefore, we designed a microfluidic platform for assessment of patient treatment response using tumor tissue slices under precisely controlled growth conditions. The optimized Cancer-on-Chip (CoC) platform maintained viability and sustained proliferation of breast and prostate tumor slices for 7 days. No major changes in tissue morphology or gene expression patterns were observed within this time frame, suggesting that the CoC system provides a reliable and effective way to probe intrinsic chemotherapeutic sensitivity of tumors. The customized CoC platform accurately predicted cisplatin and apalutamide treatment response in breast and prostate tumor xenograft models, respectively. The culture period for breast cancer could be extended up to 14 days without major changes in tissue morphology and viability. These culture characteristics enable assessment of treatment outcomes and open possibilities for detailed mechanistic studies.

Significance: The Cancer-on-Chip platform with a 6-well plate design incorporating silicon-based microfluidics can enable optimal patient-specific treatment strategies through parallel culture of multiple tumor slices and diagnostic assays using primary tumor material.

Introduction

Cancer treatment faces major challenges in defining the optimal therapy for each individual patient. While moving toward personalized treatment regimens, better stratification of patients is becoming a major hurdle. Although several molecular biomarker-driven treatment strategies have been employed for cancer therapy, they cannot reliably predict individual therapy response to chemotherapy in most cases. Therefore, *ex vivo* bioassays that can predict response of the patient would strongly aid selection of the most effective treatment for each patient aiming for optimal life expectancy and quality of life. Although cancer cell lines and animal models have been used in the past to study efficacy of chemotherapy (1–5), these models cannot easily be adapted to probe sensitivities for individual patient tumors. These preclinical models are mainly used to study general characteristics for a certain tumor type or disease stage. However, the heterogeneity of cancer and lengthy procedures to establish these models limit their use to predict individual treatment responses.

With the advent of cutting-edge molecular diagnostics tools, molecular profiling of tumors is expected to help select optimal therapies for individual patients. For example, patients with (breast) cancer with pathogenic *BRCA1*/2 mutations are homologous recombination (HR)-deficient, which makes them eligible for PARP inhibitor (PARPi) therapy (6). However, in most cases interpretation of molecular profiles for chemotherapy sensitivity prediction is not yet possible.

Direct assessment of drug response for patient stratification and personalized medicine in primary tumor tissue slice cultures may be a solution, as they contain all tumor cells, including immune cells, and maintain tissue architecture (7–9). For example, *ex vivo* culture of primary tumor tissue slices has been employed for functional analysis of HR proficiency in patients with breast cancer who may be eligible for PARPi therapy (8, 10). We have also shown that *ex vivo* treatment of prostate patient-derived xenograft (PDX) tissue slices with drugs faithfully recapitulates the *in vivo* response (11). However, long-term *ex vivo* culture (beyond 7 days) is still a challenge, probably due to mechanical stress on the tissue slices that may lead to disruption of tissue integrity and nonphysiologic behavior and/or suboptimal culture conditions (e.g., oxygen gradients that may occur in air–liquid interface cultures). Therefore, it is important to design a more physiologic *ex vivo* tissue slice culture system that allows long-term culture of tumor slices under precisely controlled conditions.

Organ-on-chip (OoC) systems encompass a combination of microfluidics, microfabrication, and tissue engineering for controlled culture

[1]Department of Molecular Genetics, Erasmus MC Cancer Institute, Erasmus University Medical Center, Rotterdam, the Netherlands. [2]Department of Cell and Molecular Biology, Manipal School of Life Sciences, Manipal Academy of Higher Education, Manipal, Karnataka, India. [3]Department of Microelectronics, Electronic Components, Technology and Materials, Delft University of Technology, Delft, the Netherlands. [4]BIOND Solutions B.V., Delft, the Netherlands. [5]Oncode Institute, Erasmus University Medical Center, Rotterdam, the Netherlands. [6]Department of Bioinformatics, Manipal School of Life Sciences, Manipal Academy of Higher Education, Manipal, Karnataka, India. [7]Philips Research, Eindhoven, the Netherlands. [8]Preclinical Intervention Unit, Mouse Clinic for Cancer and Ageing, The Netherlands Cancer Institute, Amsterdam, the Netherlands. [9]Department of Urology, Erasmus MC Cancer Institute, Erasmus University Medical Center, Rotterdam, the Netherlands.

Note: Supplementary data for this article are available at Cancer Research Online (http://cancerres.aacrjournals.org/).

Corresponding Author: Dik C. van Gent, Department of Molecular Genetics, Erasmus MC Cancer Institute, Erasmus University Medical Center, Dr. Molewaterplein 40, Rotterdam 3015GD, the Netherlands. Phone: 31-10-7043932; E-mail: d.vangent@erasmusmc.nl

Cancer Res 2022;82:510–20

doi: 10.1158/0008-5472.CAN-21-0799

of cells or tissue specimens (12, 13). It provides perfusion of media with continuous supply of nutrients to the cells, removal of waste, and the option of repeated sampling of the outflow for analysis. OoC systems have been used for preclinical studies with engineered tissue from layered cancer cell lines, spheroids, and organoids (13–15). Recently, several groups have shown that various types of primary tissue can also be maintained in a microfluidic OoC platform under controlled flow of media (16–20).

Chemotherapy sensitivity assessment of (breast) tumors requires development of a reproducible culture system for the biological material. Ideally, the assay should use live material that closely resembles the original tumor and probes sensitivity in a reproducible way. Three-dimensional tissue culturing with continuous perfusion in a controlled environment appears to be the best solution for this purpose. The challenge is to design the optimal Cancer-on-Chip (CoC) platform, sufficiently representative for the *in vivo* cancer tissue that needs to be treated and allowing long-term culture of complex 3D tumor tissue without gross change in viability or tissue characteristics. Ideally, such a system should allow direct evaluation of treatment response by microscopic imaging and liquid sampling-based analysis. In this study, we describe a novel microfluidic CoC platform, which is based on an easy-to-use 6-well plate design supporting silicon-based microfluidic chips. These chips are more flexible than culture systems using glass because they allow easy integration of sensors for detection of pH, metabolite screening, and oxygen sensing. Moreover, a silicon-based design allows parallelization as it is based on semiconductor technology improving scalability, reproducibility, and possibility for cost-effective large-scale production. One of the applications of our novel CoC platform is in personalized medicine by enabling culturing of tumor tissue slices *in vitro* under precisely controlled conditions to predict *in vivo* tumor response of individual patients to therapy. We here show that the novel CoC platform allows tumor-slice culturing using PDXs and that this culture system faithfully mimicked the *in vivo* response to cisplatin therapy for breast cancer and apalutamide treatment for prostate cancer.

Materials and Methods

Design of the CoC platform

We have developed a microfluidic chip that consists of microfluidic channels embedded in a polydimethylsiloxane (PDMS) film (**Fig. 1A**; Supplementary Fig. S1). The PDMS film with the microfluidics is supported by a silicon (Si) frame, which includes a well facing the PDMS layer. The frame also includes two openings, an inlet and outlet, to the channels in the film (**Fig. 1B**). Each channel (400 μm wide) is fully isolated and confined in the PDMS film and in contact with the open well via an array of micropores with 4 μmol/L pore size and 4% porosity (4.54×10^5 pores cm^{-2}). The organotypic tissue slices were cultured in a closed version of a BIOND plate, the COMPlate (**Fig. 1C** and **D**). This plate enables connection between multiple microfluidic chips with the tissue slices and the perfused media provided through a pumping system with controlled flow (Fluigent Deutschland GmbH, Germany). The plate can accommodate up to 6 chips in parallel in a 6-well format. Each chip is sealed between the bottom and top plates with its own inflow and outflow channels, allowing the possibility to take out one of the chips individually during the test without interfering with the others (**Fig. 1D**). The top plate with 4-mm x 4-mm width and 3.5-mm height provides the compartment to flow the media from the top channel to preserve the viability of the multilayered tissue. Additionally, the top plate provides an interface between the inlet and outlet of the chip to enable the diffusion of media through the membrane that supports the tissue. The top plate has four standard 1/4″ microfluidic fittings to connect to external pumping systems (**Fig. 1D**). The bottom part is designed to guarantee microscope compatibility and oxygenation through the PDMS of the window openings underneath the chips (**Fig. 1E**; ref. 21). Detailed description on fabrication of the BIOND microfluidic chip can be found in the supplementary method. From now on, we refer to the combination of microfluidic chip and tissue slice culture interface as CoC platform.

Simulation of fluid-flow and analysis of shear stress

The microfluidic chip and COMPlate were modelled using the finite element method–based software COMSOL Multiphysics. The modelling was specifically made for solving the Navier–Stokes equations under steady-state conditions given the pressure-driven system used in practical experiments.

PDX models

Breast cancer PDX tumors have been described before (2). Mouse experiments were approved by the Netherlands Cancer Institute animal experiments committee. We have used a breast cancer PDX model established from a triple-negative breast tumor with a HR deficiency caused by *BRCA1* mutations (c.2210delC/2329delC) resulting in cisplatin-sensitive tumors (2).

A cisplatin-resistant subline was created by repeated cisplatin treatment (T250), as described previously (2). The prostate cancer PDX model0 PC82 was established from a radical prostatectomy specimen of an otherwise untreated patient previously (22). The PDX is androgen dependent and antiandrogen therapies, such as apalutamide treatment, cause immediate tumor regression (22, 23).

Tumor tissue slice culture in CoC platform

To establish the tumor tissue slice culture protocol in our CoC platform, breast and prostate cancer PDX tumors were used. For each experiment, breast PDX tumor was sliced in 300-μm–thick slices using a Leica VT1200S vibratome and placed directly in 3 mL customized breast medium within 3 hours after the tumor was removed from the mouse, as described previously (8). Breast PDX tissue slices were either cultured in 3 mL customized culture medium in 6-well standard plates on an orbital shaker at 60 rpm (referred to as *ex vivo* culture) or in the CoC platform in duplicates (Supplementary Fig S2A). Prostate PDX tumor PC82 tissue slices were processed as per previously established protocol (11) and cultured using serum-free aDMEM/F12 K medium with synthetic androgen R1881 in *ex vivo* culture and in the CoC platform. For the CoC platform, breast and prostate PDX tissue slices were attached to the PDMS membrane using Mebiol hydrogel (Cosmobio), a biocompatible thermo-reversible copolymer of poly(N-isopropylacrylamide) and poly(ethylene glycol) providing additional protection of the tumor tissue slice from shear force and allowing gas and nutrient exchange. The complete system was assembled and connected to a FLPG Plus pumping system for continuous perfusion (**Fig. 1F**). The flow rate was maintained by a pressure-driven microfluidic flow control system (Fluigent MFCS^{TM}-EZ) and monitored by flowrate sensors (Fluigent FLOW UNIT-S) using Fluigent Microfluidic Automation Tool (MAT) for the entire culture period. PDX tissue slices were perfused with an inlet flowrate of 5 μL/minute through the top and bottom channels. Both *ex vivo* and CoC tissue culture were performed in a humidified 5% CO_2 atmosphere at 37°C and medium was changed every 3 days for up to 2 weeks. Tissue slices were removed from the chip at various time points (day 7 and day 14), kept on prechilled

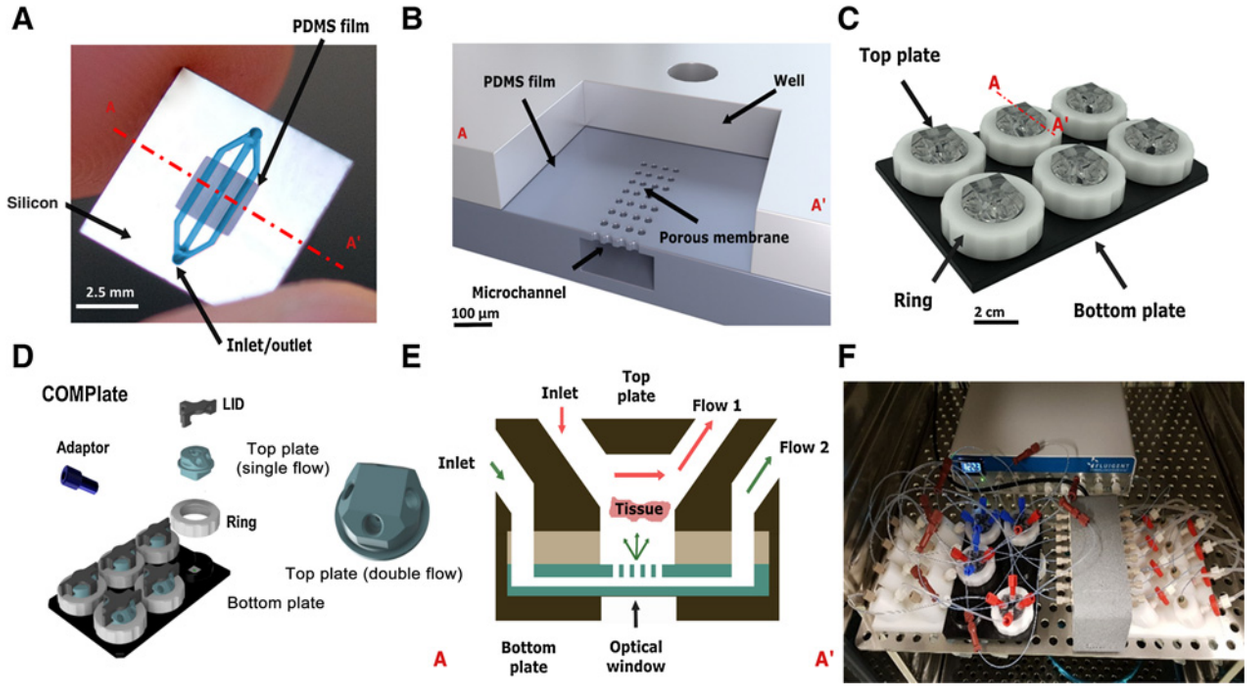

Figure. 1.

Microfluidic CoC platform design and overview. **A,** Top view of the microfluidic chip illustrating its components: the PDMS film in which the microfluidics are embedded, the silicon frame, which includes the inlet and outlet to the channels in the film. Scale bar, 2.5 mm. **B,** Vertical cross-section of the microfluidic chip. The PDMS film with the microfluidic channel is supported by a silicon frame, which includes a well facing the PDMS layer. The microchannel and the well are separated by a microporous PDMS membrane (4-µm pore size). Scale bar, 100 µm. **C,** Representation of the CoC platform. The platform, which consists of a bottom and a top plate, houses the microfluidic chip and allows for its connection to external fluidics. The ring is used to seal the system, to maintain adequate pressure for the controlled flow within the fluidic channel, and to minimize leakage. Scale bar, 2 cm. **D,** Accessories of the CoC platform with two different top plate designs. We have used double flow for this study. **E,** Cross-section of CoC illustrating the diffusion and perfusion toward the tissue slice. First the tissue slice is added to the microfluidic chip, which is in turn sandwiched between the top and bottom plates and connected to the external pump. Breast PDX tissue slices were perfused with an inlet flowrate of 5 µL/minute through the top and bottom channels. **F,** CoC platform connected to Fluigent Microfluidic flow control system that was further connected to flowrate sensors (Fluigent FLOW UNIT-S) using Fluigent MAT for the entire culture period.

medium at 0°C for 5 minutes to liquify the hydrogel and transferred to fresh medium containing 3 µg/mL 5-ethynyl-2′-deoxyuridine (EdU; Invitrogen) during the last 2 hours before fixation. Subsequently, the tissue slices were fixed in 10% neutral buffered formalin for at least 24 hours at room temperature. Tumor slices were embedded in paraffin and 4-µm sections were made for microscopic analysis.

Treatment of PDX tissue slices in CoC platform

Cisplatin response was evaluated using cisplatin-sensitive breast PDX tumors and cisplatin-resistant breast PDX tumors. Breast tumor tissue slices from cisplatin-sensitive breast PDX tumors ($n = 3$) and cisplatin-resistant breast PDX tumors ($n = 3$) were cultured in *ex vivo* 6-well plates and the CoC platform, with or without cisplatin (5 µg/mL) in medium for 72 hours. Subsequently, tissue slices were harvested and processed as described above (Supplementary Fig. S2B).

In addition, the CoC platform was tested for the treatment response of prostate PDX against the antiandrogen apalutamide. PC82 tumor ($n = 1$) tissue slices were cultured in duplicates using serum-free aDMEM/F12 K medium with synthetic androgen R1881 with or without apalutamide at a final concentration of 1 µmol/L for 7 days in CoC platform. After 7 days, PC82 PDX tissue slices were harvested and processed for staining and image analysis as described above (Supplementary Fig. S2B).

Tissue slice staining and analysis

Hematoxylin and eosin staining was performed as described previously (8). To study cell proliferation, thymidine nucleoside analog EdU incorporation was assessed. EdU (3 µg/mL; Invitrogen) was added to the culture medium 2 hours before formalin fixation and its incorporation was analyzed as described previously (8). Tissue slices that had been cultured in the CoC device, were removed from the microfluidic chamber and incubated for the last 2 hours under *ex vivo* conditions with EdU as described above. Cell viability was determined using the terminal deoxynucleotidyl transferase–mediated dUTP nick end labelling (TUNEL) assay (Roche Life Sciences; ref. 8). To quantify EdU and TUNEL staining, 10 random images (×400 magnification) from different locations of the section were captured from each tumor tissue slice section that was cultured in *ex vivo* 6-well plate or CoC platform using a Leica fluorescence microscope (DM4000b) to represent the tumor tissue slice heterogeneity. After fixation, paraffin embedding, and sectioning, sections were deparaffinized in xylene followed by rehydration in graded alcohols. Antigen retrieval was performed with target retrieval buffer, pH 6 (Dako). For diaminobenzidine (DAB) staining, endogenous peroxidase activity was blocked with 3% hydrogen peroxide solution in methanol for 20 minutes at room temperature. Primary antibody anti-Pan Cytokeratin (AE1/AE3; Santa Cruz Biotechnology, sc-81714) was diluted in blocking buffer (1/500 in 5% BSA in PBS) and applied to the sections for 90

minutes at room temperature and a secondary Alexa Fluor 488 antibody conjugate was used to detect the first antibody. The Ki67 antibody (ab16667, Abcam) was diluted in blocking buffer (1/200 in 5% BSA in PBS) and applied to the sections at 4°C overnight. Ki67 was detected with horseradish peroxidase (HRP)-conjugated anti-rabbit IgG secondary antibody (Dako) at a 1:100 dilution for 1 hour at room temperature. Ki67-positive cells were visualized using DAB staining kit (Agilent) followed by counterstaining with hematoxylin. TUNEL, EdU, and DAPI images were analyzed automatically using previously published methods (10). Quantitative image-based cytometry single-cell analysis (QIBC) was performed for immunofluorescence analysis of cell cycle using anti-geminin (Proteintech Group 10802–1-AP, 1:400) in PDXs cultured in *ex vivo* and CoC platform conditions. The analysis of the imaging data has been conducted using customized pipelines in Cell Profiler (24). Nuclei were detected using the DAPI signal and filtered for intensity, size, perimeter, and solidity to exclude nontumor and stromal cells. The intensity in 594 channel was corrected with the background intensity. The selection of geminin-/DAPI-positive cells were performed based on the mean intensity of the geminin signal for individual nucleus. For the quantification of 53bp1 foci per nucleus, a mask was generated in the 53BP1 channel using the detection of local intensity maxima, with a threshold set for spot radius and intensity. Clumped spots were split using the shape features. The desired quantified values for each nucleus were exported to the Tibco Spotfire software and to the GraphPad Prism 8 for generation of scatter diagrams and bar chart respectively.

For prostate PDX tumor slices, primary androgen receptor (AR) antibody (M4074, 1/200, SPRING Bioscience), diluted in blocking buffer, was applied to the sections at 4°C overnight. Subsequently, slides were incubated with HRP-conjugated anti-rabbit IgG secondary antibody (Dako) at a 1:100 dilution for 1 hour at room temperature. AR-positive cells were visualized using DAB staining kit (Agilent) followed by counterstaining with hematoxylin. Imaging of AR staining was performed using a light microscope (Olympus). For quantification of AR expression, four fields (×200 magnification) from each prostate PDX tumor slice section were captured and analyzed using Image J software as described previously (11). To assess DNA damage repair, 53BP1 (anti-rabbit, 1/1000, Novus Biologicals) staining was performed in PDX tumor tissue slices treated with cisplatin as described previously (25).

RNA isolation and sequencing

Whole transcriptome analysis was performed using RNA sequencing (RNA-seq) using three independent breast cancer PDX tumors. RNA was isolated from formalin-fixed, paraffin-embedded (FFPE) tissue using RNeasy FFPE kit (Qiagen) according to the manufacturer's protocol. Quality and quantity of the RNA was assessed using a NanoDrop 2000 spectrophotometer (Thermo Fisher Scientific). RNA libraries for mRNA sequencing were prepared from FFPE tissue using Kapa mRNA Hyperprep kit (Roche Life Sciences) with unique dual indices from Integrated DNA Technologies (IDT). Sequencing was performed using 2 × 150 bp paired-end method on the Illumina Novaseq 6000 platform.

Bioinformatics analysis

The FastQ files obtained were analyzed for QC using the FastQC program. Adapter trimming and removal of homo-polymers were performed using FLEXBAR and reads less than 25 bases were discarded (26).The trimmed and processed FastQC files were separately aligned to human and mouse genomes (GRCh38 and GRCm38 versions) downloaded from GENCODE respectively using HISAT2 (a splice aware aligner; ref. 27). Samtools and PICARD programs were used on the aligned files to obtain the mapping statistics and other RNA-seq metrics (28). We used XenofilteR, an R-package to separate mouse reads from the aligned human sequence reads (29). Expression analysis was performed for both human and mouse mapped reads using StringTie using the reference only approach and the gene abundance tables were obtained (30). We used the feature Counts program to generate the count table for differential expression analysis (31). Bioconductor package edgeR was used for differential expression analysis (32). Gene ontology and pathway analysis of differentially expressed genes were performed using metascape (www.metascape.org), Ingenuity Pathway Analysis (IPA) for canonical pathway analysis.

Pathway analysis

qRT-PCR–based pathway analysis tests were performed using three independent breast PDX tumors with each cultured at day 0, up to day 7, and up to day 14 in *ex vivo* and CoC platform. Functional activity of the estrogen receptor (ER), AR, PI3K, and MAPK growth factor pathways, Hedgehog (HH), Notch, and TGFβ cell signaling pathways was measured using qRT-PCR–based pathway analysis tests using FFPE derived RNA from each breast PDX tumor group cultured in *ex vivo* and CoC platform (33). Functional pathway activity of individual pathways was analyzed based on the interpretation of mRNA levels of target genes of the pathway-associated transcription factors (www.Philips.com/Oncosignal). Pathway activity scores are presented on a normalized 0 to 100 scale, as described previously (34–36).

Statistical analysis

Results are expressed as the mean ± SEM in bar graph. Mann–Whitney test was used to analyze the differences between two groups. Statistical analysis and generation of graphs was performed using GraphPad Prism 8.0. P value < 0.05 was considered statistically significant.

Results

CoC workflow

Development of methods to predict chemotherapy sensitivity of tumors requires a robust and reproducible culture system for the biological material. Ideally, the assay should use live material that closely resembles the original tumor and probes sensitivity. Three-dimensional (3D) tissue culturing with continuous perfusion in a controlled environment appears to be the best solution for this purpose. Therefore, we designed a novel platform with a microfluidic chip and tissue culture interface for OoC cultures with 3D tissue specimens (**Fig. 1A** and **B**). The platform was designed to accommodate tissue slices that can be used for cancer (chemo)therapy response assays. Tissue slices were immobilized using a thermoreversible hydrogel that allows easy removal of the biological specimen after cooling on ice. The tissue culture interface was made in a 6-well plate format, which hosts the microfluidic chips with tumor tissue slices (**Fig. 1C**). The design of the COMPlate allows individual tumor slices to be cultured and analyzed independently. The top plate is designed to provide option for single flow or double flow of the media (**Fig. 1D**). Each well provides enough space to accommodate the tissue slice and allows growth over time. The tissue slices can be maintained while removing waste products and replenishing nutrients through constant perfusion and diffusion from the microchannel and the top part of the interface (**Fig. 1E**). Moreover, oxygenation of the tissue slices is

augmented by gas exchange through the PDMS layer of the optical window (**Fig. 1E**). The entire CoC platform was connected to a Fluigent Microfluidic flow control system to monitor fluid flow rate inside each individual well during the entire culture period (**Fig. 1F**).

Modeling of shear stress in the CoC platform

The CoC geometry consists of three microfluidic channels (90 μmol/L thick, 400 μmol/L wide) with a porous membrane (4 μmol/L pore size), the well (4 mm × 4 mm, 3.5-mm height) and the corresponding inlets and outlets for perfusion of media (Supplementary Fig. S3A shows the situation for one microfluidic bottom channel). As the precise characteristics were not available for all components, we modelled the microfluidics set up such that maximally expected shear force in the most unfavorable case was determined. The tissue slice was modelled as a porous material with permeability 3×10^{-12} m^2 (37). The hydrogel used to fix the tissue slices was modelled as a water permeable rectangular region (Supplementary Fig. S3B; ref. 38). The medium was modelled as an incompressible fluid with a density of 1,000 kg/m^3 and a viscosity of 1.0 mPa-s. The inlet flow rate on top and bottom was set to 5 μL/minute. The outlets were set as open boundaries at environmental pressure. The boundaries defining the microchannel, pores and well were set as walls with a no-slip condition. The domains were then meshed with a highly dense (3.5 million elements) and average quality (0.8%) mesh. The model was solved in static conditions to obtain the velocity field and shear stress distributions close to the tissue. The velocity and stress fields shown correspond to the well and areas where the tissue is located during experiments (Supplementary Fig. S3C and S3D). Simulations showed that under the conditions set for the inlet flow (5 μL/minute), a laminar flow was obtained with the average velocity (0.4–1 μm/second) around the tissue within the range of physiologic interstitial flow (37, 39). The highest shear stress experienced by the tissue would be very low (approximately 10^{-5} dyn/cm^2), even below physiologic shear stresses detected in lymphatic capillaries (40). Further simulations were performed to show the fluid flow across the membrane inside the CoC platform (Supplementary Fig. S4). We conclude that this low level of shear stress will most probably not influence biological functions in a nonphysiologic way.

Treatment response of PDX tumors in the CoC platform

In order to use the CoC platform for drug sensitivity assessment, the first important question is whether treatment responses in the CoC platform are predictive for therapy response *in vivo*. We tested response to cisplatin treatment using cisplatin-sensitive and cisplatin-resistant breast cancer PDX tumors (three biological replicates of each). Cytokeratin staining showed that most cells in the breast PDX tumor tissue slices were tumor cells with minimal numbers of stromal cells at the start of the treatment, suggesting tissue responses are mainly caused by tumor cell sensitivities (Supplementary Fig S5). Untreated tumor slices at day 0 and at day 7 in the CoC platform showed Ki67-positive tumor epithelial cells and negative mouse stromal cells, suggesting that the CoC platform culture method retains the tumor-associated cell morphology and proliferative capacity, which is essential for treatment response analysis (Supplementary Fig. S6). Tissue slices cultured under regular *ex vivo* conditions and in the CoC platform were treated with cisplatin for 3 days and evaluated for proliferation and cell death. Cisplatin-sensitive tumor slices in the CoC platform showed a significant increase in TUNEL-positive (apoptotic) cells and a significant drop in EdU-positive (replicating) cells upon cisplatin treatment (**Fig. 2A** and **B**). As expected, the cisplatin-resistant PDX tissue slices did not show any significant change in EdU and TUNEL signal when compared with untreated controls (**Fig. 2C** and **D**). Cisplatin treatment for 72 hours caused a much higher accumulation of 53BP1 foci in cisplatin-sensitive PDX than in cisplatin-resistant tumor slices (**Fig. 2E** and **F**), presumably as a result of failed repair of the DNA damage in the sensitive model. Cultures in the CoC platform showed a response to cisplatin treatment that correlated well with the known tumor response *in vivo* (2), as well as in *ex vivo* cultures (**Fig. 2B** and **D**; Supplementary Fig. S7A and S7B). Interestingly, breast PDX cultured in the CoC platform showed a stronger response to cisplatin treatment than the *ex vivo* culture method, suggesting that the CoC platform provides more optimal drug delivery into the tumor slices than the *ex vivo* culture method (Supplementary Fig. S8).

The androgen-dependent prostate tumor PC82 was used to assess the performance of the CoC platform in a completely different tumor type. Tumor tissue slices were cultured for 7 days with or without the antiandrogen apalutamide. We found significantly reduced AR expression, increased TUNEL-positive cells, and a significant decrease in EdU-positive cells after apalutamide exposure, very similar to the effect of antiandrogen treatment *in vivo* (41) and in *ex vivo* cultures (**Fig. 3**; Supplementary Fig. S7C). In summary, the CoC cultures recapitulate tumor responses for two different treatments in breast and prostate tumor models with known sensitivities *in vivo*.

Comparison of long-term tumor tissue slice culture in *ex vivo* and in CoC platform

Ideally, culture time should be extended to allow studies into therapy responses that require incubation times extending beyond 1 week (such as therapy resistance development or clonal outgrowths). One of the main limitations of the *ex vivo* culture appeared to be the maximum culture time preserving optimal proliferative capacity and tissue architecture. Breast tumor slices from five independent PDX tumors were cultured in the CoC platform for up to 14 days. In parallel, tissue slices from the same breast PDX tumors were cultured in the *ex vivo* 6-well plate. After 7 days of culture, we observed similar cellular proliferation rate in CoC (fraction of EdU-positive cells) as in day 0 (25.05% vs. 23.06%), but a slightly slower proliferation in the *ex vivo* condition (23.06% vs. 19.50%; **Fig. 4A** and **B**). TUNEL staining showed slightly increased cell death *ex vivo* than in CoC at day 7 (3.5% versus 2.2%; **Fig. 4A** and **B**). Interestingly, this pattern was more pronounced in extended cultures for 14 days, which revealed better preservation of tumor tissue architecture and cell proliferation in the CoC platform than in the *ex vivo* culture system. We found a much higher fraction of EdU-positive cells in CoC than *ex vivo* (20.65% vs. 8.06%, $P < 0.0001$; **Fig. 4C**). Moreover, analysis of cell death by TUNEL staining showed 17.03% TUNEL-positive cells in the *ex vivo* condition and only 6% in the CoC platform ($P < 0.0001$; **Fig. 4C**). Comparatively, in CoC, we observe very little change in cell proliferation between day 0 (25%) and day 14 tumor slices (20.65%; **Fig. 4C**).

This was confirmed by immunofluorescent staining for geminin, as marker for S and G2 phase cells, where we observed a significant decrease in geminin-positive cells *ex vivo* at day 7 when compared with day 0 PDX tumors (31.65% vs. 19.20%; $P = 0.0002$), while no significant differences could be observed between day 7 CoC and day 0 (31.65% vs. 27.20%; **Fig. 4D–F**), suggesting slightly slower cellular proliferation of tumors cultured in *ex vivo* condition in comparison with CoC (**Fig. 4D–F**). These data indicate that the CoC platform provides better culture conditions for extended (beyond 7 days) culture times of tumor tissue slices than the *ex vivo* system and that there may already be subtle differences between both culture methods even after 7 days.

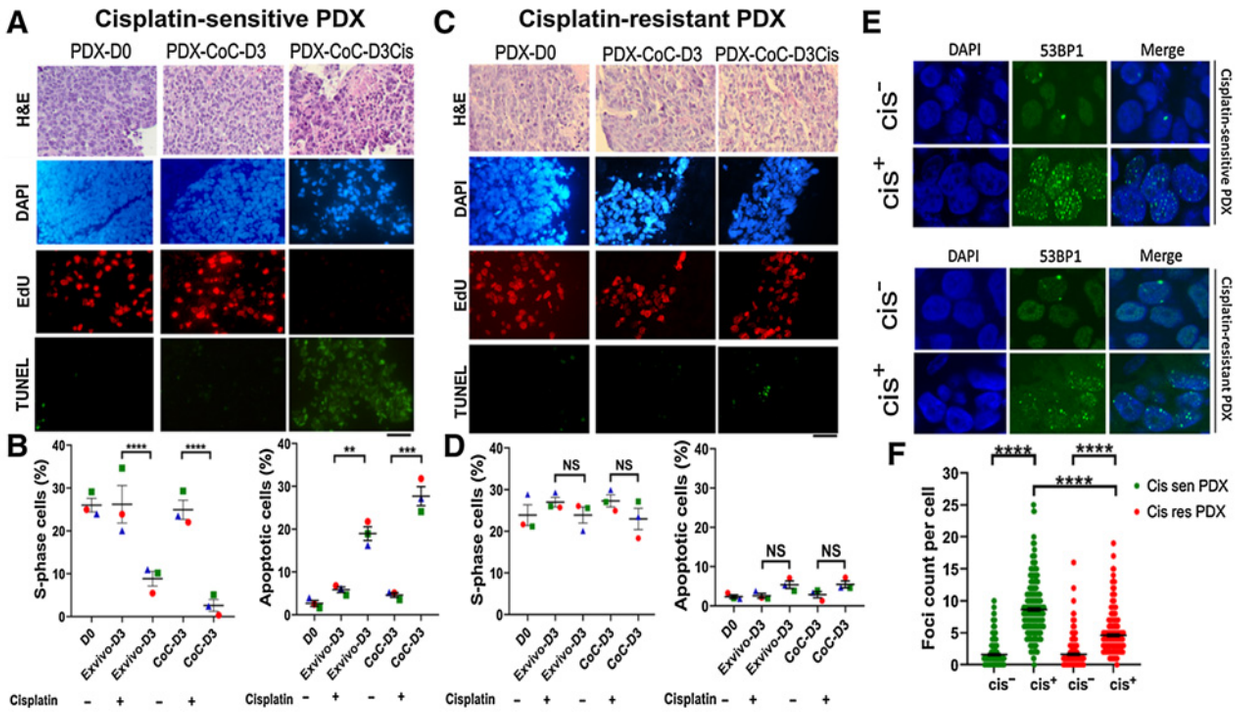

Figure 2.

Prediction of therapy response using cisplatin-sensitive and -resistant PDX in *ex vivo* and CoC platform. Three cisplatin-sensitive and three cisplatin-resistant breast PDX tumors were used in three independent experiments to study cisplatin response in *ex vivo* 6-well plate culture and CoC platform. Cisplatin-sensitive and -resistant PDX tumor tissue slices were exposed to 5 μg/mL cisplatin for 3 days and evaluated for cell proliferation (EdU incorporation, red nuclei) and apoptosis (TUNEL staining, green nuclei). DAPI stains all nuclei blue. **A,** Representative EdU and TUNEL staining of cisplatin-sensitive breast PDX. **B,** Quantification of the fraction of EdU-positive and TUNEL-positive cells showing breast PDXs ($n = 3$) were sensitive to cisplatin. **C,** Representative EdU and TUNEL staining of cisplatin-resistant breast PDX. **D,** Quantification of the fraction of EdU-positive and TUNEL-positive cells showing breast PDXs ($n = 3$) were insensitive to cisplatin therapy, thereby validating the application of CoC for therapy response for patient tumors. Ten fields of view were quantified from each breast PDX slice. Each point in the graph represents one breast PDX sample and SEM is indicated for all three tumors in the three independent experiments. Scale bar, 50 μm. **E,** Analysis of DNA damage response in cisplatin-sensitive and -resistant PDX treated with cisplatin. Cisplatin treatment induced more double-strand breaks in cisplatin-sensitive PDX than in cisplatin-resistant PDX. Scale bar 50 μmol/L. **F,** Scatter plot showing 53BP1 foci count per cell in cisplatin-sensitive and -resistant PDX. Averages and SEM are indicated. Cis, cisplatin; cis res, cisplatin-resistant; cis sen, cisplatin-sensitive; H&E, hematoxylin and eosin. NS, not significant; **, $P < 0.01$; ***, $P < 0.001$; ****, $P < 0.0001$.

Gene expression analysis

In order to characterize the CoC culture for more subtle gene expression changes, we performed RT-PCR–based analysis of tumor-specific genetic pathways from breast PDX tumors cultured *ex vivo* ($n = 3$) and in the CoC platform ($n = 3$). We did not observe any statistically significant changes in these pathways (**Fig. 5A**; Supplementary Table S1), suggesting that both culture conditions did not induce any major changes in growth characteristics of the tumor.

We extended this analysis to whole transcriptome sequencing using breast PDX tumors ($n = 3$). Differentially expressed genes at day 7 *ex vivo* and day 7 and 14 CoC culture conditions were selected based on log fold change ($\log_{FC}$) > 1.5, FDR < 0.1 for significantly upregulated genes and $\log_{FC}$ <- 1.5, FDR < 0.1 for significantly downregulated human and mouse genes (**Fig. 5B**; Supplementary Tables S2 and S3). In this analysis, human genes represent expression in tumor cells, while the mouse genes are derived from stromal cells. We observed 150 human genes differentially expressed in *ex vivo* day 7 tumor slices that was significantly more than the 30 differentially expressed human genes in CoC day 7 and 14 human genes in CoC day 14 (Supplementary Table S2). These upregulated human tumor genes ($\log_{FC} > 1.5$, FDR < 0.1) in *ex vivo* culture condition are significantly enriched in several immune signaling pathways (**Fig. 5C**), one of which is the IFN signaling pathway (Supplementary Table S4). Consistent with this, IPA showed activation of cellular immune response in the *ex vivo* tumor slice culture condition (**Fig. 5D**). In line with these findings, gene expression analysis of mouse stromal genes showed down-regulation of collagen genes (*Col3a1*, *Col6a2*, *Col15a1*) in the *ex vivo* culture (Supplementary Table S3), which is a known effect of IFNγ signaling (42).

To investigate the reason for the reduction in cell-cycle progression and the increase in apoptosis, we performed 53BP1 immunostaining to analyze for DNA damage status in tumor slices at day 0 and day 7 under both culture conditions. We observed cells with one large focus, as well as cells with multiple small foci under both *ex vivo* and CoC conditions (**Fig. 5E**). However, there was a significantly higher increase in DNA damage in tumors cultured *ex vivo* condition than in CoC (16.38% vs. 11.34%; $P = 0.04$; **Fig. 5F**). We therefore conclude that the *ex vivo* (but not the CoC) culture condition induced immune activation and that more DNA damage is present after 7 days of *ex vivo culture*, making the CoC system a more faithful representation of the original tumor and the preferred system for studying therapy responses.

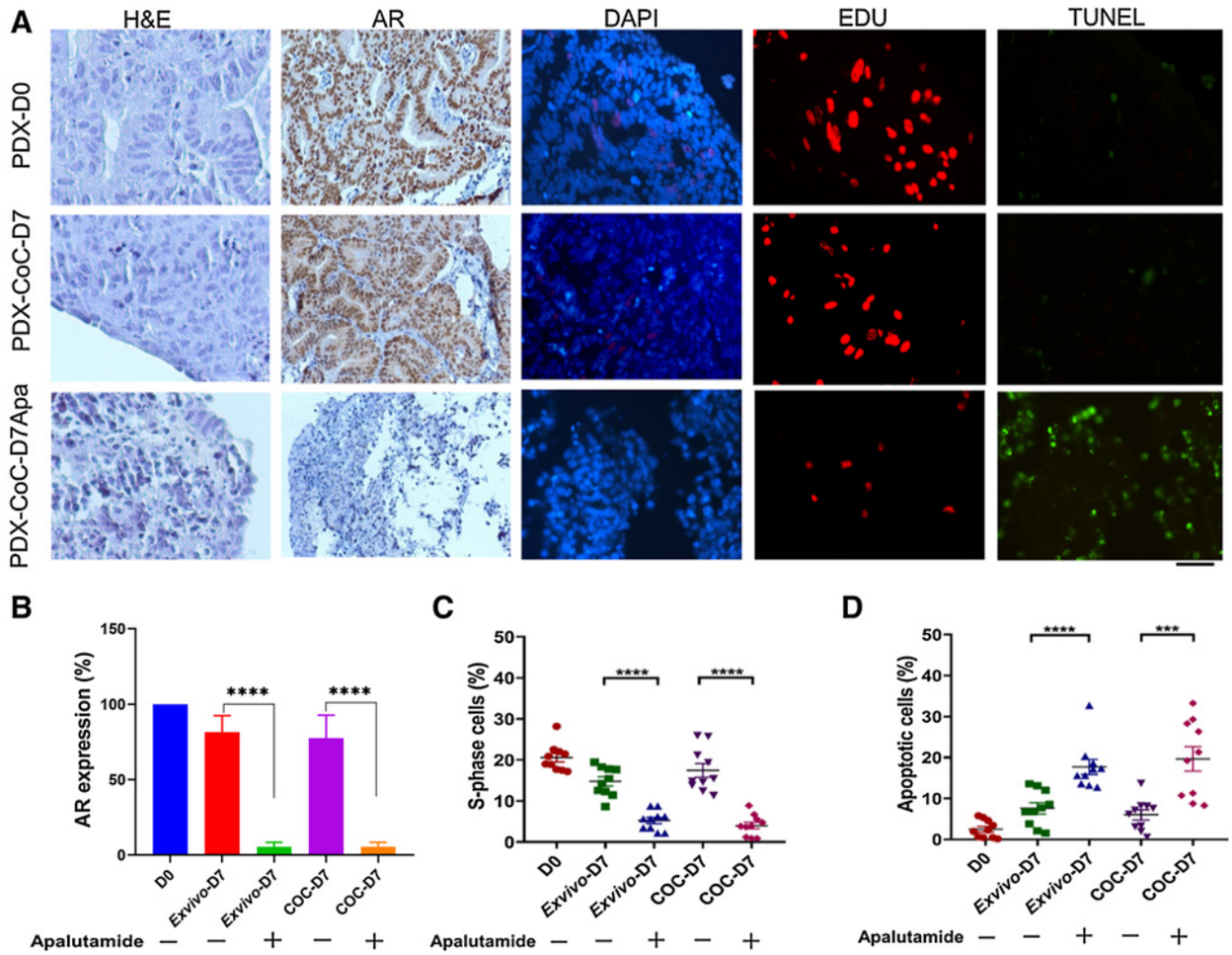

Figure 3.

Response to apalutamide treatment in CoC platform. **A,** PC82 tumor tissue slices cultured with apalutamide for 7 days and evaluated for AR expression, cell proliferation (EdU incorporation, red nuclei), and apoptosis (TUNEL staining, green nuclei). AR staining for PC82 tissue slice sections at day 0, day 7 *ex vivo* culture condition, and CoC platform with and without apalutamide treatment. DAPI stains all nuclei blue. H&E, hematoxylin and eosin. Scale bar, 50 μm. **B,** Quantification of the AR expression in prostate PDX slices cultured in *ex vivo* and CoC platform. **C** and **D,** Apalutamide treatment showed a significant increase in TUNEL-positive cells and significant decrease in EdU-positive cells when compared with untreated tumor slices in our CoC platform. Ten fields of view were quantified per prostate PDX slice. Each point in the graph represents one image field and SEM is indicated for 10 fields. D7, day 7; D0, day 0. ***, $P < 0.001$; ****, $P < 0.0001$.

Discussion

We previously developed methods to culture precision cut breast tumor slices *ex vivo* (8). Here, we describe the design of a diagnostic CoC platform to grow tumor tissue slices for prolonged periods of time, which permits investigation of chemotherapy responses in a controlled environment. Defining features of this microfluidic system are: (i) relatively large (tumor) tissue slices can be loaded (ii), flow of culture media both above and under the tissue slice to sustain constant delivery of nutrients and gasses and removal of waste products (iii), mainly silicon-based components (iv), standard 6-well format, allowing parallelization, and (v) options for imaging and media outflow analysis to follow tissue responses in time.

These features make this device particularly suitable for diagnostic investigation of fresh tumor biopsies, which requires the option to load a relatively large piece of tumor material in the microfluidic device and relatively constant growth conditions throughout the tissue specimen. The top and bottom flow minimize gradients throughout a relatively thick tissue slice and the fixation of this slice on the membrane using a thermoreversible hydrogel allows both easy loading and disassembly, while also reducing tear forces on the tissue. Previously published similar systems either used only bottom flow (16, 43–45) or perfusion through the slice (18, 20). Our design not only allows efficient perfusion but can also be adapted to mimic a blood vessel (by coating the bottom channel with endothelial cells) or create gradients by using different top and bottom flow media (e.g., by adding the therapeutic agent only in the bottom channel).

Furthermore, silicon-based components reduce absorption of (chemotherapeutic) agents. This is especially important when using PDMS-based devices and hydrophobic compounds (46). In the current version of the device, PDMS is still used for the membrane supporting the tumor slice, but this can also be replaced by other materials, such as Polyethylene terephthalate (PET) and Polystyrene (PS), thermoplastics that are molded with techniques that might be coupled to the last stages of silicon-based fabrication processes, helping

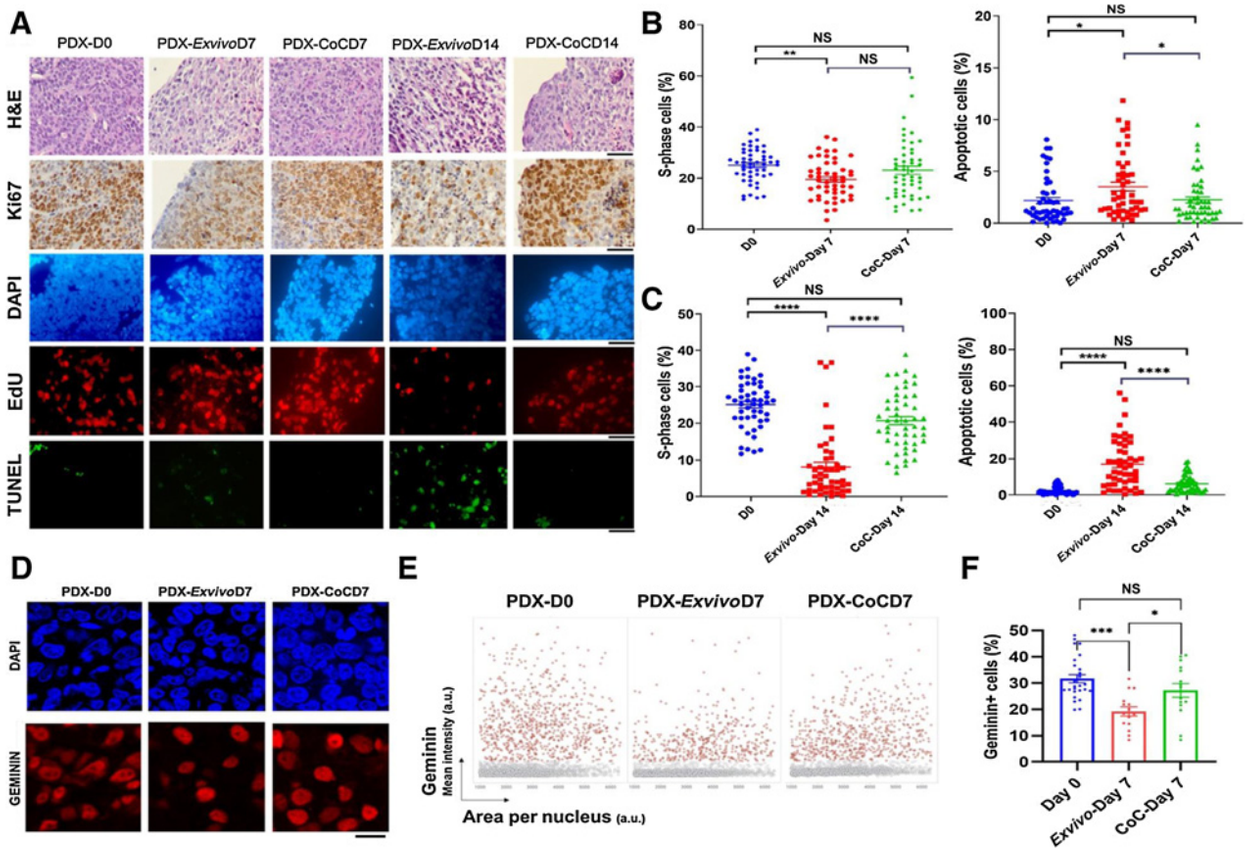

Figure 4.

Breast PDX tumor tissue slices cultured in *ex vivo* condition and in CoC platform for up to 14 days. **A,** We used five independent breast PDX tumors in five independent experiments to establish optimized culture condition for tumor slices in our CoC platform. From each breast PDX tumor, tissue slices were cultured in *ex vivo* 6-well plate and CoC device for up to 14 days and evaluated for tissue morphology [hematoxylin and eosin (H&E) staining], DAPI (blue nuclei), proliferation (EdU incorporation, red nuclei), Ki67 (brown nuclei), and apoptosis (TUNEL staining, green nuclei). Scale bar, 50 μm. **B** and **C,** Quantification of the fraction of EdU-positive and TUNEL-positive cells for 5 breast PDX tissue slices (derived from individual PDX tumors) cultured for up to day 7 (**B**) and day 14 (**C**). For each breast PDX tumor and each condition, tissue slices were imaged, and ten random fields of view were quantified from each breast PDX slice. Each data point in the graph represents one image field. Error bar represents the SEM for the five independent tumors performed in five independent experiments. **D,** Representative image showing breast PDX tumors ($n = 3$) labeled with geminin (red nuclei) and DAPI (blue nuclei). Scale bar, 50 μm. **E,** QIBC analysis of three independent breast PDX tumors with more than 3,000 cells analyzed for each are shown in each condition. **F,** Quantification of geminin-positive cells showed CoC at day 7 had similar cell proliferation profile as in day 0 than *ex vivo* condition. Error bar, SEM. NS, not significant; D0, day 0; D7, day 7, D14, day 14. NS, not significant; *, $P < 0.05$; **, $P < 0.01$; ***, $P < 0.001$; ****, $P < 0.0001$.

to overcome the intrinsic absorption limitations but guaranteeing to maintain manufacturability.

Options for parallelization and analysis of live tumor samples make this device usable for a broad spectrum of experimental designs. The current design allows testing of six tissue slices individually; each unit can be assembled and disassembled without disturbing the other samples, allowing analysis of different time points in the same run. Outflow media are collected individually, allowing analysis of their composition over time, e.g., by isolating extracellular vesicles and investigation of their mRNA content. Furthermore, the CoC device presented here is an evolution of the Cytostretch platform that can be equipped with electrodes and other sensors to allow real time measurement of additional parameters, such as oxygen, pH, and temperature (47, 48).The optical window allows visual (microscopic) detection of tissue samples during the culture period. In the current design, working distance and optical performance of the PDMS window are not optimal for live microscopic imaging. These parameters may be improved in a new version by using alternative materials, such as a glass window instead of PDMS.

The growth conditions in the CoC platform maintain original growth characteristics of the tumor better than the previously described *ex vivo* culture system. Proliferation was maintained for a longer period of time (14 days compared with 7 days) with less apoptosis induction at day 14. Although proliferation was maintained for 7 days in both systems, careful analysis of gene expression revealed some important changes in the *ex vivo* condition that were not detected in the CoC cultures. Tumor cells showed increased IFN signaling at day 7 *ex vivo*, but not in the CoC device, suggesting increased stress levels in the tissue that could translate to changes in therapy sensitivity and nonphysiologic activation of immune responses. In line with the increased stress levels *ex vivo*, tumor cells showed a subtle difference in cell cycle profile and induction of DNA damage at day 7. Although the induction of DNA damage was also observed in the CoC culture condition, it was more pronounced *ex vivo*. We observed many cells

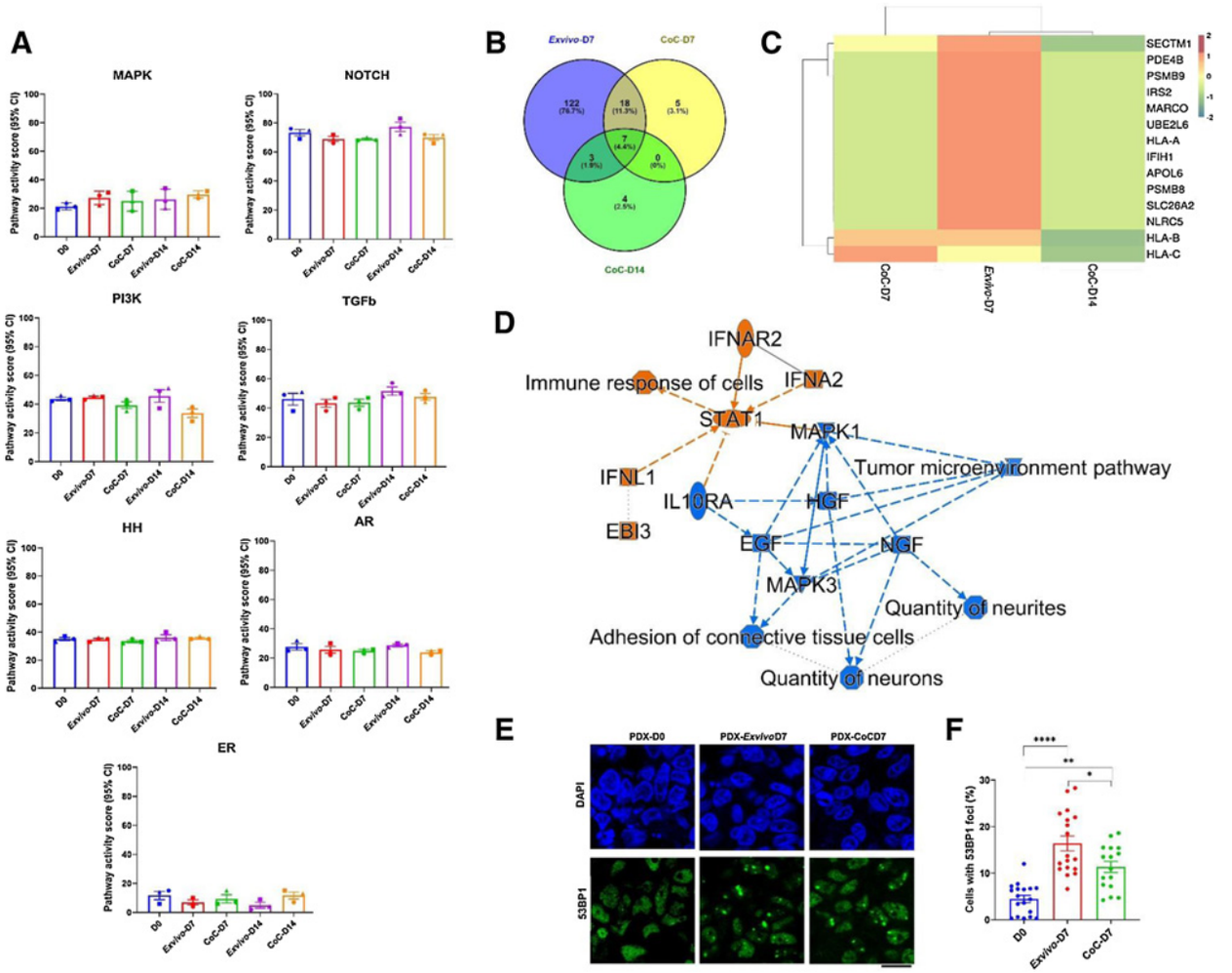

Figure 5.

Gene expression analysis of breast PDX tumor cultured in *ex vivo* and CoC platform. Three independent breast PDX tumors (P1, P2, and P3) were used for analysis of pathway activity using OncoSignal and RNA-seq for whole mRNA expression analysis. **A,** Seven major pathways were analyzed (ER, AR, PI3K, and MAPK growth factor pathways, HH, Notch, and TGFβ cell signaling pathways) using OncoSignal. Pathway activity scores are presented on a normalized scale of 0 to 100. Error bars, SEM. Mann–Whitney test of seven pathway activity across PDX tumor slices (day 0, day 7, day 14) in *ex vivo* and CoC condition did not show any statistically significant change. **B,** Venn diagram showing differentially expressed human (*ex vivo*-D7, CoC-D7, and CoC-D14) genes ($\log_{FC} > 1.5$ or $\log_{FC} \leq 1.5$, FDR < 0.1) in PDX tumors at day 7 and day 14 in *ex vivo* and CoC platform when compared with day 0 PDX tumors. **C,** Heatmap diagram showing IFN signaling pathway gene expression at different days in *ex vivo* and in CoC platform culture condition. **D,** Network diagram showing top ranked networks significantly enriched in immune signaling and tumor microenvironment ($P < 0.05$) exclusively in day 7 *ex vivo* culture condition. Orange, predicted activation of the pathways (Z score > 2); blue, predicted inhibition (Z score ≤2). **E,** Representative image showing 53BP1 staining in breast PDX tumors cultured at day 0, day 7 *ex vivo* and CoC condition. DAPI staining is shown as blue nuclei. Scale bar, 50 μm. **F,** Bar chart showing the percentage of cells with 53BP1 foci. Error bar, SEM for the three independent PDX tumor samples. D0, day 0; D7, day 7, D14, day 14. *, $P < 0.05$; **, $P < 0.01$; ****, $P < 0.0001$.

with a single large accumulation of 53BP1 protein. A similar phenomenon has been observed before in cells and was shown to be due to replication stress (49), suggesting that the culture conditions presented here led to similar replication problems. We suspect that the oxygen concentration may play a role in this (20% ambient oxygen compared with less than 5% in most tissues). One possible solution to reduce the basal DNA damage levels could be lowering the oxygen concentration in the CoC platform. The deterioration of tumor tissue was further enhanced at day 14, when we observed extensive morphologic changes along with increased cell death in PDX tumor slices in the *ex vivo* condition. The CoC cultures were much less affected and did not show a significant difference in proliferation or apoptosis.

Previously, tissue slice culture methods in air-liquid interfaces have been reported (50–52). These systems are good for mimicking lung or skin tissues. However, it is not desirable for assessment of sensitivities in tumors, which should not be exposed to high oxygen levels. Especially treatment with DNA damaging agents should not be combined with high oxygen levels, as this causes oxidative DNA damage, which may form a gradient from the outer layers of the tumor slice to the center where oxygen levels will be much lower. This would hamper analysis of responses to the DNA damaging agent under investigation. However, also other treatment responses could be influenced by oxidative (DNA) damage in such culture systems. Our observation that 53BP1 foci were increased after 7 days of culture

suggests that oxidative damage may indeed be an important factor to be controlled even better than we did in the experiments presented here.

Gene expression analysis showed that immune responses (such as IFN signaling) were affected under *ex vivo* conditions, but not in the CoC platform. Therefore, we expect that the CoC device will be especially suitable to study immune responses in the tumor. Furthermore, immune cells can be added in a controlled way by inflow through top or bottom channel. The obvious advantage over mouse models is the option to add human immune system components and measure responses in real time.

We developed a microfluidic CoC platform that maintained cell viability, proliferation, and tissue morphology for at least 14 days for breast cancer PDX slices. It faithfully predicted cisplatin therapy response for breast cancer and antiandrogen treatment response for prostate cancer PDX tumor slices. Further validation of its potential as an *in vitro* diagnostic test for therapy selection will require clinical validation using biopsies of patient tumors that are going to be treated with the same chemotherapy. Although the present study focused on breast and prostate cancer PDX models, the CoC platform may be applied to other solid tumors, as well. With its ease of use and flexibility to operate with minimum footprint, our CoC platform is a versatile tool for *ex vivo* studies for functional genomics, drug screening, and personalized medicine.

Authors' Disclosures

W.F. Quiros-Solano reports a patent for PCT/NL2017/050492 issued; in addition, W.F. Quiros-Solano is cofounder and holds equity in BIOND Solutions B.V. A. Othman is a Field Application Scientist at BIOND Solutions B.V. C. Silvestri reports a patent for PCT/NL2017/050492 issued; in addition, C. Silvestri is cofounder and Chief Executive Officer, and holds equity in BIOND Solutions B.V. N. Gaio reports grants from ECSEL Joint Undertaking during the conduct of the study; in addition, N. Gaio has a patent for PCT/NL2017/050492 issued; and is a cofounder and Chief Technology Officer, and holds equity in BIOND Solutions B.V. R. Kanaar reports grants from Dutch Research Council (NWO) and grants from Gravitation program CancerGenomiCs.nl from the NWO and is part of the Oncode Institute, which is partly financed by the Dutch Cancer Society during the conduct of the study. D.C. van Gent reports grants from Dutch Cancer Foundation (KWF) and grants from Dutch Research Council (NWO) during the conduct of the study. No disclosures were reported by the other authors.

Authors' Contributions

S. Chakrabarty: Data curation, software, formal analysis, validation, investigation, methodology, writing–original draft, writing–review and editing. **W.F. Quiros-Solano:** Resources, data curation, formal analysis, investigation, methodology, writing–original draft. **M.M.P. Kuijten:** Data curation, formal analysis, methodology, writing–original draft. **B. Haspels:** Data curation, formal analysis, investigation. **S. Mallya:** Data curation, software, formal analysis. **C.S.Y. Lo:** Software, formal analysis, visualization. **A. Othman:** Writing–review and editing. **C. Silvestri:** Writing–review and editing. **A. van de Stolpe:** Data curation, formal analysis, methodology. **N. Gaio:** Data curation, formal analysis, investigation, methodology, writing–review and editing. **H. Odijk:** Data curation, formal analysis. **M. van de Ven:** Data curation. **C.M.A. de Ridder:** Data curation. **W.M. van Weerden:** Resources, formal analysis, investigation, methodology, writing–review and editing. **J. Jonkers:** Writing–review and editing. **R. Dekker:** Funding acquisition, writing–review and editing. **N. Taneja:** Software, formal analysis, writing–review and editing. **R. Kanaar:** Conceptualization, funding acquisition, project administration, writing–review and editing. **D.C. van Gent:** Conceptualization, formal analysis, supervision, funding acquisition, investigation, writing–original draft, writing–review and editing.

Acknowledgments

The authors thank the people from the Preclinical Intervention Unit of the Mouse Clinic for Cancer and Ageing (MCCA) at the NKI for performing the PDX tumor outgrowth.

This work was supported by the KWF grant KWF11011, by the Gravitation program CancerGenomiCs.nl from the Dutch Research Council (NWO), the Oncode Institute, which is partly financed by the Dutch Cancer Society and the NWO (Building Blocks of Life grant 737.016.011). Part of this work is supported by Moore4Medical project funded by the ECSEL Joint Undertaking under grant number H2020-ECSEL-2019-IA-876190 (https://moore4medical.eu/).

The costs of publication of this article were defrayed in part by the payment of page charges. This article must therefore be hereby marked *advertisement* in accordance with 18 U.S.C. Section 1734 solely to indicate this fact.

Received March 11, 2021; revised August 31, 2021; accepted November 30, 2021; published first December 6, 2021.

References

1. Stebbing J, Paz K, Schwartz GK, Wexler LH, Maki R, Pollock RE, et al. Patient-derived xenografts for individualized care in advanced sarcoma. Cancer 2014; 120:2006–15.
2. Ter Brugge P, Kristel P, van der Burg E, Boon U, de Maaker M, Lips E, et al. Mechanisms of therapy resistance in patient-derived xenograft models of BRCA1-deficient breast cancer. J Natl Cancer Inst 2016;108:djw148.
3. Vlachogiannis G, Hedayat S, Vatsiou A, Jamin Y, Fernandez-Mateos J, Khan K, et al. Patient-derived organoids model treatment response of metastatic gastrointestinal cancers. Science 2018;359:920–6.
4. Malaney P, Nicosia SV, Dave V. One mouse, one patient paradigm: New avatars of personalized cancer therapy. Cancer Lett 2014;344:1–12.
5. Zhang Y, Wang L, Gao P, Sun Z, Li N, Lu Y, et al. ISL1 promotes cancer progression and inhibits cisplatin sensitivity in triple-negative breast cancer cells. Int J Mol Med 2018;42:2343–52.
6. Rottenberg S, Jaspers JE, Kersbergen A, van der Burg E, Nygren AOH, Zander SAL, et al. High sensitivity of BRCA1-deficient mammary tumors to the PARP inhibitor AZD2281 alone and in combination with platinum drugs. Proc Natl Acad Sci USA. 2008;105:17079–84.
7. Seo YD, Jiang X, Sullivan KM, Jalikis FG, Smythe KS, Abbasi A, et al. Mobilization of CD8+ T cells via CXCR4 blockade facilitates PD-1 checkpoint therapy in human pancreatic cancer. Clin Cancer Res 2019; 25:3934–45.
8. Naipal KA, Verkaik NS, Sanchez H, van Deurzen CH, den Bakker MA, Hoeijmakers JH, et al. Tumor slice culture system to assess drug response of primary breast cancer. BMC Cancer 2016;16:78.
9. Martin SZ, Wagner DC, Hörner N, Horst D, Lang H, Tagscherer KE, et al. Ex vivo tissue slice culture system to measure drug-response rates of hepatic metastatic colorectal cancer. BMC Cancer 2019;19:1030.
10. Meijer TG, Verkaik NS, Sieuwerts AM, van Riet J, Naipal KAT, van Deurzen CHM, et al. Functional ex vivo assay reveals homologous recombination deficiency in breast cancer beyond BRCA gene defects. Clin Cancer Res 2018; 24:6277–87.
11. Zhang W, van Weerden WM, de Ridder CMA, Erkens-Schulze S, Schonfeld E, Meijer TG, et al. Ex vivo treatment of prostate tumor tissue recapitulates in vivo therapy response. Prostate 2019;79:390–402.
12. Jeon JS, Bersini S, Gilardi M, Dubini G, Charest JL, Moretti M, et al. Human 3D vascularized organotypic microfluidic assays to study breast cancer cell extravasation. Proc Natl Acad Sci U S A 2015;112:214–9.
13. Shirure VS, Bi Y, Curtis MB, Lezia A, Goedegebuure MM, Goedegebuure SP, et al. Tumor-on-a-chip platform to investigate progression and drug sensitivity in cell lines and patient-derived organoids. Lab Chip 2018;18:3687–702.
14. Ayuso JM, Virumbrates-Munoz M, McMinn PH, Rehman S, Gomez I, Karim MR, et al. Tumor-on-a-chip: a microfluidic model to study cell response to environmental gradients. Lab Chip 2019;19:3461–71.
15. Holliday DL, Brouilette KT, Markert A, Gordon LA, Jones JL. Novel multicellular organotypic models of normal and malignant breast: tools for dissecting the role of the microenvironment in breast cancer progression. Breast Cancer Res 2009; 11:R3.
16. Hattersley SM, Sylvester DC, Dyer CE, Stafford ND, Haswell SJ, Greenman J. A microfluidic system for testing the responses of head and neck squamous cell

carcinoma tissue biopsies to treatment with chemotherapy drugs. Ann Biomed Eng 2012;40:1277–88.
17. Astolfi M, Peant B, Lateef MA, Rousset N, Kendall-Dupont J, Carmona E, et al. Micro-dissected tumor tissues on chip: an ex vivo method for drug testing and personalized therapy. Lab Chip 2016;16:312–25.
18. Riley A, Green V, Cheah R, McKenzie G, Karsai L, England J, et al. A novel microfluidic device capable of maintaining functional thyroid carcinoma specimens ex vivo provides a new drug screening platform. BMC Cancer 2019;19:259.
19. Cao X, Ashfaq R, Cheng F, Maharjan S, Li J, Ying GL, et al. A tumor-on-a-chip system with bioprinted blood and lymphatic vessel pair. Adv Funct Mater 2019; 29:1807173.
20. Kennedy R, Kuvshinov D, Sdrolia A, Kuvshinova E, Hilton K, Crank S, et al. A patient tumour-on-a-chip system for personalised investigation of radiotherapy based treatment regimens. Sci Rep 2019;9:6327.
21. Firpo G, Angeli E, Repetto L, Valbusa U. Permeability thickness dependence of polydimethylsiloxane (PDMS) membranes. J Membr Sci 2015;481:1–8.
22. van Weerden WM, de Ridder CM, Verdaasdonk CL, Romijn JC, van der Kwast TH, Schröder FH, et al. Development of seven new human prostate tumor xenograft models and their histopathological characterization. Am J Pathol 1996; 149:1055–62.
23. Navone NM, van Weerden WM, Vessella RL, Williams ED, Wang Y, Isaacs JT, et al. Movember GAP1 PDX project: An international collection of serially transplantable prostate cancer patient-derived xenograft (PDX) models. Prostate 2018;78:1262–82.
24. Lo CSY, van Toorn M, Gaggioli V, Dias MP, Zhu Y, Manolika EM, et al. SMARCAD1-mediated active replication fork stability maintains genome integrity. Sci Adv 2021;7:eabe7804.
25. Zhang W, Liao C-Y, Chtatou H, Incrocci L, van Gent DC, van Weerden WM, et al. Apalutamide sensitizes prostate cancer to ionizing radiation via inhibition of non-homologous end-joining DNA repair. Cancers (Basel) 2019;11:1593.
26. Dodt M, Roehr JT, Ahmed R, Dieterich C. FLEXBAR-flexible barcode and adapter processing for next-generation sequencing platforms. Biology (Basel) 2012;1:895–905.
27. Kim D, Paggi JM, Park C, Bennett C, Salzberg SL. Graph-based genome alignment and genotyping with HISAT2 and HISAT-genotype. Nat Biotechnol 2019;37:907–15.
28. Li H, Handsaker B, Wysoker A, Fennell T, Ruan J, Homer N, et al. The sequence alignment/map format and SAMtools. Bioinformatics 2009;25:2078–9.
29. Kluin RJC, Kemper K, Kuilman T, de Ruiter JR, Iyer V, Forment JV, et al. XenofilteR: computational deconvolution of mouse and human reads in tumor xenograft sequence data. BMC Bioinformatics 2018;19:366.
30. Pertea M, Pertea GM, Antonescu CM, Chang TC, Mendell JT, Salzberg SL. StringTie enables improved reconstruction of a transcriptome from RNA-seq reads. Nat Biotechnol 2015;33:290–5.
31. Liao Y, Smyth GK, Shi W. featureCounts: an efficient general purpose program for assigning sequence reads to genomic features. Bioinformatics 2014;30: 923–30.
32. Robinson MD, McCarthy DJ, Smyth GK. edgeR: a Bioconductor package for differential expression analysis of digital gene expression data. Bioinformatics 2010;26:139–40.
33. Canté-Barrett K, Holtzer L, van Ooijen H, Hagelaar R, Cordo' V, Verhaegh W, et al. A molecular test for quantifying functional Notch signaling pathway activity in human cancer. Cancers. 2020;12:3142.
34. Inda MA, Blok EJ, Kuppen PJK, Charehbili A, den Biezen-Timmermans EC, van Brussel A, et al. Estrogen receptor pathway activity score to predict clinical response or resistance to neo-adjuvant endocrine therapy in primary breast cancer. Mol Cancer Ther 2020;19:680–9.
35. Verhaegh W, van Ooijen H, Inda MA, Hatzis P, Versteeg R, Smid M, et al. Selection of personalized patient therapy through the use of knowledge-based computational models that identify tumor-driving signal transduction pathways. Cancer Res 2014;74:2936–45.
36. van de Stolpe A. Quantitative measurement of functional activity of the PI3K signaling pathway in cancer. Cancers (Basel) 2019;11:293.
37. Shim S, Belanger MC, Harris AR, Munson JM, Pompano RR. Two-way communication between ex vivo tissues on a microfluidic chip: application to tumor-lymph node interaction. Lab Chip 2019;19:1013–26.
38. Fujiyabu T, Li X, Shibayama M, Chung U, Sakai T. Permeation of water through hydrogels with controlled network structure. Macromolecules 2017;50:9411–6.
39. Munson JM, Shieh AC. Interstitial fluid flow in cancer: implications for disease progression and treatment. Cancer Manag Res 2014;6:317–28.
40. Pisano M, Triacca V, Barbee KA, Swartz MA. An in vitro model of the tumor-lymphatic microenvironment with simultaneous transendothelial and luminal flows reveals mechanisms of flow enhanced invasion. Integr Biol (Camb) 2015;7: 525–33.
41. van Weerden WM, van Steenbrugge GJ, van Kreuningen A, Moerings EP, de Jong FH, Schröder FH. Assessment of the critical level of androgen for growth response of transplantable human prostatic carcinoma (PC-82) in nude mice. J Urol 1991;145:631–4.
42. Diaz A, Jiménez SA. Interferon-gamma regulates collagen and fibronectin gene expression by transcriptional and post-transcriptional mechanisms. Int J Biochem Cell Biol 1997;29:251–60.
43. Chang TC, Mikheev AM, Huynh W, Monnat RJ, Rostomily RC., Folch A. Parallel microfluidic chemosensitivity testing on individual slice cultures. Lab Chip 2014; 14:4540–51.
44. Horowitz LF, Rodriguez AD, Dereli-Korkut Z, Lin R, Castro K, Mikheev AM, et al. Multiplexed drug testing of tumor slices using a microfluidic platform. npj Precision Oncology 2020;4:1–13.
45. Rodriguez AD, Horowitz LF, Castro K, Kenerson H, Bhattacharjee N, Gandhe G, et al. A microfluidic platform for functional testing of cancer drugs on intact tumor slices. Lab Chip 2020;20:1658–75.
46. Shirure VS, George SC. Design considerations to minimize the impact of drug absorption in polymer-based organ-on-a-chip platforms. Lab Chip 2017;17: 681–90.
47. Gaio N, Van Meer B, Quirós Solano W, Bergers L, Van de Stolpe A, Mummery C, et al. Cytostretch, an organ-on-chip platform. Micromachines 2016;7:120.
48. da Ponte RM, Gaio N, van Zeijl H, Vollebregt S, Dijkstra P, Dekker R, et al. Monolithic integration of a smart temperature sensor on a modular silicon-based organ-on-a-chip device. Sens Actuators, A 2021;317:112439.
49. Lukas C, Savic V, Bekker-Jensen S, Doil C, Neumann B, Sølvhøj Pedersen R, et al. 53BP1 nuclear bodies form around DNA lesions generated by mitotic transmission of chromosomes under replication stress. Nat Cell Biol 2011;13:243–53.
50. Muruganandan S, Fan X, Dhal S, Nayak NR. Development of A 3D tissue slice culture model for the study of human endometrial repair and regeneration. Biomolecules 2020;10:136.
51. Schopow N, Kallendrusch S, Gong S, Rapp F, Körfer J, Gericke M, et al. Examination of ex-vivo viability of human adipose tissue slice culture. PLoS One 2020;15:e0233152.
52. Cao X, Coyle JP, Xiong R, Wang Y, Heflich RH, Ren B, et al. Invited review: human air-liquid-interface organotypic airway tissue models derived from primary tracheobronchial epithelial cells—overview and perspectives. In Vitro Cell Dev Biol Anim 2021;57:104–32.